www.rericjournal.ait.ac.th

Modified Method to Determine Small Signal Stability Region Boundary for Power System with DFIG

Avrin Nur Widiastuti*, Sasongko Pramono Hadi*, [1], and Sarjiya Sarjiya*, #

ARTICLE INFO

Article history:
Received 28 October 2022
Received in revised form
07 July 2023
Accepted 14 July 2023

Keywords:
Automatic voltage regulator (AVR)
Doubly-fed induction generator (DFIG)
Modal analysis
Power system stability
Small signal stability region (SSSR)

ABSTRACT

Despite providing advantages to the grid, large-scale wind power penetration causes system stability problems. To solve this issue, some researchers have applied stability analysis to a wide area of operation, namely the small signal stability region (SSSR) boundary. However, some boundary points of the SSSR result in a positive real part of the eigenvalues, indicating unstable conditions. Therefore, a study that guarantees stability in the power system is necessary. This study proposes a modified method for determining the SingSR boundary, which guarantees stability within a wide range of operational areas and ensures that every boundary point has a negative real part of the eigenvalues. This study used a four-bus test system modeled in DIgSILENT PowerFactory and a type 3 wind turbine generator, the doubly-fed induction generator (DFIG). This research also investigated the effects of the automatic voltage regulator (AVR) and DFIG operation type using the modified method developed. The results of the simulation demonstrate that the proposed method successfully guaranteed stability at each SSSR boundary point, as indicated by the negative real part of all eigenvalues. This study presents a new approach for investigating the wind power integration's effect on small signal stability.

1. INTRODUCTION

Embracing environmentally friendly renewable energy sources is one approach to reducing the pollution caused by burning fossil fuels to generate electricity. In recent years, wind energy has become the most commonly used renewable energy resource due to its technological experience and global availability [1]–[3]. However, connecting renewable energy resources to the power system establishes a new type of power source that differs from conventional synchronous generators (SG) [3]. Furthermore, high penetration of wind power causes a decrease in system inertia due to the displacement of the SG [4], hence, significantly affecting the dynamic performance of a power system [3], [4]. Therefore, an investigation on how wind power penetration influences the stability of the power system is necessitated.

The most common and broadly used wind turbine generator is type 3, the doubly-fed induction generator (DFIG) [2]–[7]. The eigenvalue analysis approach is generally applied to assess the grid's stability condition with small disturbances [8]–[15]. Some studies have suggested that integrating DFIG may lead to grid instability [8]–[10]. Conversely, other findings have mentioned that adding DFIG improves the grid's stability [12], [13]. Following this, the different operating conditions examined in the reviewed studies led to this disparate outcome. Research [8] discussed the grid-connected DFIG's small signal stability study employing modal and time-domain analysis.

AVR on a SG has a significant effect on grid stability. It provides the fundamental voltage control of the SG [11]. Consequently, its impact on the grid stability with DFIG integrated needs further analysis. Research on the effects of AVR on system stability has been carried out by [10], [11], [14], [15]. Research [10] demonstrated the usefulness of AVR and PSS in the electrical power system connected to the DFIG. However, there was only one type of AVR used in the study. In comparison, the differences in system stability when using various types of AVR were discussed in [11]. However, most references only employed one specific operating condition, and their results do not broadly discuss other working points [8]–[15]. Due to the high percentage of wind power integration in the power system, a wide-ranging operation points stability analysis is needed.

Furthermore, enhancement in voltage stability can be attained by managing a DFIG wind turbine's reactive power output control capability [4]. The influence of reactive power support on system stability with DFIG was observed in some studies [7], [9]. The DFIG usually only injects active power, implying that it does not contribute to the reactive power of the network. In

* Department of Electrical and Information Engineering. Faculty of Engineering, Universitas Gadjah Mada, Special Region of Yogyakarta 55281, Indonesia.

Center for Energy Studies, Universitas Gadjah Mada, Special Region of Yogyakarta 55281, Indonesia.

[1]Corresponding author:
Tel: +62 0274 552305.
Fax: +60 0274 547506.
Email: sasongko@ugm.ac.id

contrast, reactive power significantly affects the stability of the grid, especially in voltage stability [16]. Therefore, further research is required to determine how the DFIG operating type affects stability in the power system.

In research [17]–[21], the technique of establishing a small signal stability region (SSSR) boundary to determine stability over a wide operating range was introduced. The boundary of the SSSR was determined by the point set of Hopf bifurcation (HB) [17]–[20]. When the complex eigenvalues cross the imaginary axis, the system encounters the HB, which is related to oscillatory instability [19], [20]. The investigation of HB was conducted by looking for various points where the system's eigenvalues reached instability [19]. Furthermore, research [19] compared the effects of wind power connection and synchronous generator coupling strength on small signal stability using the SSSR boundary. Earlier studies revealed that some eigenvalues are zero or very small positive values [19], [20]. This situation threatens the system because stability is only obtained when the real eigenvalues are negative.

This study aims to modify an existing method used to determine the new SSSR boundary by considering the generator's operation points prior to system instability. The primary purpose of the new SSSR boundary is to guarantee the system's stability. The criteria for stability is that the eigenvalues must be less than zero or placed in the left half of the complex plane [13]. This criteria is achieved by modifying the step to find the points of stability limits and ensuring that the real part of all eigenvalues is negative. This method guarantees the stability of every operating point inside the SSSR boundary. Furthermore, this study used the modified method to obtain the new SSSR boundary to investigate the effects of various AVR and DFIG operations on small signal stability at various operating points.

This study used a four-bus system modeled in DIgSILENT PowerFactory 2018. It also utilized the Python programming language to calculate the SSSR boundary. Employing a modified method for calculating the boundary of the SSSR, this study produced a set of stability points at various DFIG penetration levels, which led to achieving stability over a wide operating range. The new SSSR boundary obtained in this study is valuable for electrical operators in regulating the power output of each generator.

2. SMALL SIGNAL STABILITY REGION OF POWER SYSTEM WITH CONNECTED DFIG

A basic understanding of small signal stability, SSSR boundary, and DFIG theory are required to obtain the SSSR boundary of a system with connected DFIG. The following section also provides an explanation of the AVR to support the simulation.

2.1 Small Signal Stability

The ability of the system to preserve stability when minor disruptions occur is known as small signal stability [22]. Because the disruption is minimal, the system can be linearized. The modal or eigenvalue analysis method is frequently used in analyzing small signal stability [8]–[15], [23]. Furthermore, Equation 1 shows the equation for determining the eigenvalue.

$$\dot{x} = Ax + Bu$$
$$y = Cx + Du \quad (1)$$

$$\lambda = \sigma \pm j\omega \quad (2)$$

The values of λ that satisfy the characteristic equation are assigned as the eigenvalues of matrix A [10], [23]. The eigenvalue amount corresponds to the number of first-order differential equations used in the simulation to describe the system [10]. The eigenvalues of matrix A in Equation 1 determine the power system stability [21]. Eigenvalue may consist of real and imaginary parts, with the complex number always in a conjugate pair, as presented in Equation 2. The damping is determined by the real part of the eigenvalue, whereas the oscillation frequency is determined by the imaginary part [3].

Stability analysis uses the dominant eigenvalue mode to determine the system's stability. The dominant mode is the largest real component of the eigenvalue, located furthest right on the real axis. A system is considered stable when all eigenvalues' real parts are negative [23]. Conversely, the positive real part of the eigenvalues indicates that the system is unstable.

2.2 Small Signal Stability Region (SSSR) Boundary

The SSSR boundary comprises a set of operating points indicating the system's stability limits [19], [20]. This boundary shows the whole system's range of critical operations; hence, evaluations are conducted in comprehensive assessment [19], [20]. The SSSR boundary method is widely used for conventional electrical systems without renewable energy. Also, when the DFIG has highly penetrated the power system, the stability analysis method with the SSSR boundary becomes more accurate.

According to theory [19] and [20], the saddle-node bifurcation (SNB), HB, and singularity-induced bifurcation (SIB) make up the SSSR boundary. The HB is linked to the oscillatory instability of the system since it physically reveals a pair of conjugate eigenvalues passing the imaginary axis. The SSSR boundary composed of HB is the primary subject of this research.

In steady states, the real components of eigenvalues are fewer than zero. Therefore, a system is said to be in a stable state if and only if all of its real parts of eigenvalues are negative. However, the system's stability can change according to its parameters because if the parameters vary, the HB may rise. In addition, when two conjugate complex eigenvalues traverse the imaginary axis, HB occurs [19].

Compared to other studies [19], [20], this research modifies the calculation of the SSSR boundary by looking for a point of stability before instability occurs. Therefore, the boundary was created before the HB happened. This study guarantees that every operating point on the SSSR boundary has a negative real part of eigenvalues. This research presents a modified approach

to establish the SSSR boundary resulting in a thorough analysis and ensuring the system's stability. This study is also to acquire the SSSR boundary on the active power generator in the system.

Figure 1 represents the SSSR boundary where the active power injections P1 from generator 1 and P2 from generator 2 establish the two-dimensional SSSR boundary. P1 and P2 represent the SG output and the DFIG output. The shaded and unshaded areas also indicate stable and unstable regions, respectively. Hence, if one of the power plants has an operating point beyond the stable boundary, the system will experience instability. This concept can assist operators in setting the operating point of a power generation linked to the system.

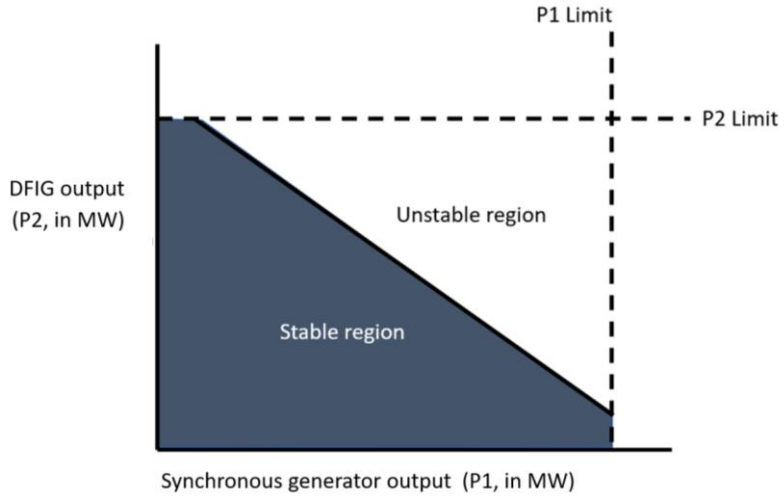

Fig. 1. Illustration of the SSSR boundary.

2.3 Doubly-Fed Induction Generator (DFIG) Model

The technology used in most modern wind turbine systems is a DFIG [2]. DFIG consists of an induction generator and a converter, as Figure 2 [24] illustrates. The induction generator's stator is directly coupled to the grid [14], [24]. The rotor, in contrast, is linked to the grid via two converters known as the rotor side converters (RSC) and grid side converters (GSC) [2], [6], [14], [24]. A DC-link capacitor exists connecting the RSC and GSC [24]. The RSC manages the power transferred by the stator, whereas the GSC is used to maintain the operating voltage of the capacitor. Therefore, both converters are in charge of managing the power delivered to the network.

Besides delivering active power, a DFIG also performs reactive power management through its converter. Furthermore, reactive power is often managed in two ways, power factor management and voltage control [25]. The power factor control maintains the power factor of the DFIG at a constant condition throughout the operation. The voltage control maintains the point common coupling (PCC) voltage corresponding to the desired values. Thus, a DFIG can be used to keep the voltage of its PCC in the permissible range through reactive power management.

Control of DFIG has an essential impact on the stability of the power system. When a terminal voltage control is used, reactive power output is controlled to reach a specific bus target voltage. With the capability to provide reactive power, DFIG can enhance system stability [9].

The wind farm is regularly made up of several wind turbines because of the limited capacity of a single wind turbine. In this study, the installed DFIG had a unit capacity of 2 MW with 120 parallel numbers; hence, the total capacity is 240 MW.

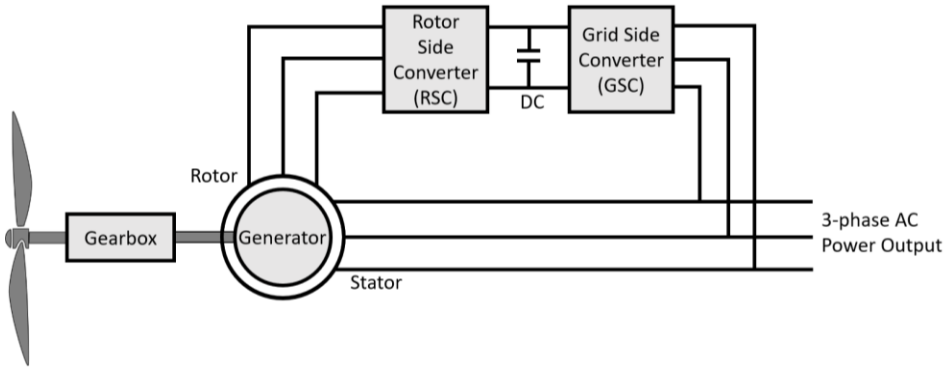

Fig. 2. DFIG wind turbine system [24].

2.4 Automatic Voltage Regulator (AVR) Model

An AVR is a device applied to maintain the terminal voltage of a synchronous generator [11],[15], and Figure 3 shows its model [26]. The figure depicts the AVR that reads the terminal voltage of the bus (Vc) and evaluates it to the reference voltage value (Vref) [26]. Its output is a field voltage (EFD) for a synchronous machine model, and the amount of the field voltage is adjusted to regulate the generator. Furthermore, the AVR of an excitation control system uses the terminal voltage error to modify the field voltage and regulate the terminal voltage magnitude. The excitation system regulates the voltage and reactive power flow and improves the stability of the power system [22].

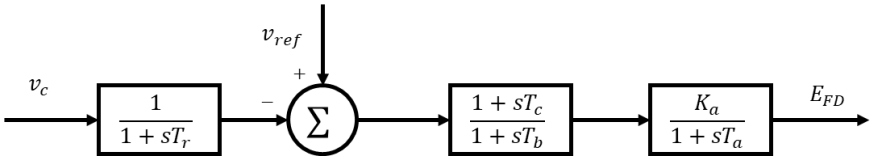

Fig. 3. Simple illustration of an AVR connected to a synchronous generator [26].

Various excitations are based on three power sources: DC, AC, and ST (static) types [27]. The DC type uses a DC generator current with a commutator as the excitation source. In contrast, the AC type uses an alternator to produce the DC the generator requires. The static type's excitation source is from a transformer and rectifier. Type DC exciter is rarely used in new synchronous machines, but many systems are still used. AC and ST are popular models compared to DC types [27].

3. MATERIALS AND METHODS

The primary purpose of this study is to establish an SSSR boundary that guarantees stability for a power system with connected DFIG. The proposed method is then applied in a four-bus test power system to determine its effectiveness.

3.1 Test System

This study used a four-bus test system, as presented in Figure 4. Other references, such as [19]–[21], also utilized similar system models. The power system contains of a synchronous generator and a wind turbine generator linked to an infinite bus through the transmission line. A large power system can be represented with an infinite bus. Thus, the interaction between synchronous generators and DFIG can be observed. With this model, the study reveals the behavior of DFIG connected to a large system. Therefore, this model is appropriate for power system stability analysis.

This study equipped the synchronous generator with an AVR that produced the required voltage, as Section 2.4 explains. Section 2.3 depicts wind generation modeled with DFIG. According to Figure 4, G1 represents an SG, and DFIG represents a wind generator.

Bus 1 was connected to a synchronous generator (G1), Bus 2 was the link between the wind turbine generator (DFIG) and network, Bus 3 was modeled as an infinite bus, and Bus 4 was linked to the DFIG.

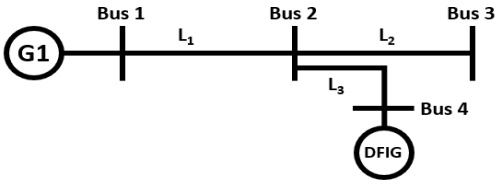

Fig. 4. Four-bus test system [19].

Table 1 shows the line and synchronous generator parameters utilized in this study. They were obtained from one of the synchronous generators on the IEEE Nine-Bus in DIgSILENT PowerFactory 2018 [19], [28]. The entire line had the same ohm/km value, with their length being the only differing attribute. Table 2 shows the line parameters [28]. Following this, the nominal voltage of the transmission system was 230 kV, and the nominal frequency was 50 Hz. Table **3.** 3 shows the installed DFIG has a unit capacity of 2 MW with 120 parallel numbers and has parameters similar to that of the DIgSILENT PowerFactory [19], [29].

Table 1. SG parameters [19], [28].

Parameter	Value
Rated Power (MW)	300
Voltage (kV)	18
Xd (pu)	1.72
Xd' (pu)	0.23
Xq (pu)	1.66
Xq' (pu)	0.378
Td0' (s)	6
Tq0' (s)	0.535

Table 2. Line parameters [28].

Parameter	L1	L2	L3
R (ohm/km)	0.044965	0.044965	0.044965
X (ohm/km)	0.38088	0.38088	0.38088
B (μS/km)	2.8166	2.8166	2.8166
Length (km)	100	200	15

Table. 3. DFIG parameters [19], [29].

Parameter	Value
Rated Power (MW)	2
Voltage (V)	690
Rs (pu)	0.01
Xs (pu)	0.1
Xm (pu)	3.5
Rr (pu)	0.01
Xr (pu)	0.1
Ht (s)	4.02
Hg (s)	0.47
Ks	80.27

3.2 Proposed Method

This study aims to improve the method of getting the SSSR boundary by evaluating the eigenvalues to guarantee the stability of the power system with DFIG integration. This research determined the stability region of the system using a modified approach to the SSSR boundary. This investigation modified the flowchart from earlier research [19] by taking the operating point of the SSSR boundary before the HB occurred. Figure 5 shows the flowchart used to find the modified SSSR boundary.

This study conducted the following procedures to obtain the SSSR boundaries using the proposed method.

1. The study considered the P1 or SG output at its maximum power of 300 MW. Simultaneously, the P2 or DFIG output worked at minimum output power (2 MW).
2. The study then ran a modal analysis to establish the eigenvalue of the system. When there was no positive real part of the eigenvalue, P2 increased by 2 MW while P1 remained unchanged.
3. This process was repeated until the HB occurred. The DFIG output (P2) had to be reduced by 2 MW (1 parallel unit of DFIG) to guarantee system stability.
4. After that, this study checked whether the real part of the dominant mode's eigenvalue was negative. This step obtained the P2 point for the first operating condition of P1 (300 MW).
5. Afterward, the study stored P1 and P2 values as one point of the SSSR boundary.
6. The algorithm searched the next point of operation by decreasing P1 output by 5 MW to accomplish the modified SSSR boundary. It means that the P1 output was 295 MW in the second simulation.
7. The simulation program searched P2 values with the previously described algorithm (steps 2-5).
8. This process was repeated until P1 reached its lower limit. Immediately after reaching the lower limit, the simulation stopped, creating the modified SSSR boundary.

The modified method makes the resulting stability analysis comprehensive for all generator operation points. Figure 4 represents this method, which was tested on a power system model. The model consisted of an SG, DFIG, and infinite bus. Figure 6 illustrates two scenarios, variations in the AVR types in SG and variations in bus types in DFIG. With these variations, the eigenvalues of matrix A in Equation 1 will change; thus, the SSSR boundary formed will be affected.

After developing the SSSR boundary, its increment (ΔP_{DFIG}) was then calculated using Equations 3 and 4. This research then calculated the magnitude of the boundary increment by comparing the active power generated by DFIG under each condition. This calculation is beneficial to discovering the best-case study that produces the widest SSSR boundary.

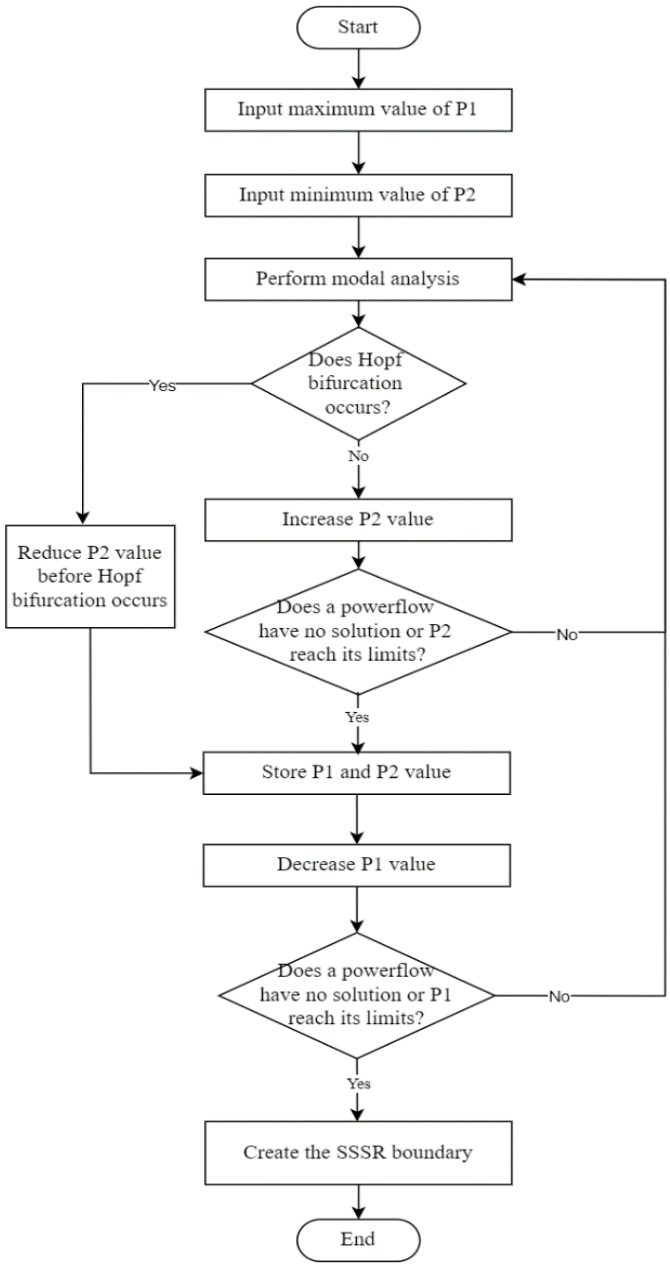

Fig. 5. Flowchart of the modified method to generate a new SSSR boundary.

The study calculated the magnitude of the SSSR boundary increment ($\overline{\Delta P_{DFIG}}$) by averaging the increase in active power generated by DFIG under each condition, as Equations (3) and (4) show. $\Delta P_{DFIG,i}$ indicates the magnitude of the DFIG's active power increment at the i-test point. Meanwhile, $P^0_{DFIG,i}$ illustrates the DFIG active power value at the initial condition at the i-test point. Notation n indicates the number of points tested in the simulation.

$$\overline{\Delta P_{DFIG}} = \frac{\sum_{i=1}^{n} \Delta P_{DFIG,i}}{n} \quad (3)$$

$$\Delta P_{DFIG,i} = \frac{P^1_{DFIG,i} - P^0_{DFIG,i}}{P^0_{DFIG,i}} \quad (4)$$

3.3 Simulation Scenarios

Figure 6 depicts the simulation scenario. The process began with the construction of a test system model. Afterward, this research ran simulations to determine the system stability with various types of AVR (on synchronous generator) and DFIG modes of operation. The study formed a modified SSSR boundary and simulated the time domain to determine the system stability under various operational conditions. This study then conducted the power system simulation using DIgSILENT PowerFactory 2018 and utilized the Python programming language to automate, establishing the modified SSSR boundary.

The synchronous generator in this study was equipped with AVR to maintain the terminal voltage value. This study used two types of AVRs, namely IEEE and EXAC. Both have similar models, but their exciter modeling uniquely distinguishes them. This study extracted the model for both AVRs from the

DIgSILENT PowerFactory library and obtained the parameter of each AVR series [30].

Each AVR type has its series; this simulation used three series from each type. This research conducted simulation cases as follows:

Case 1: SG with no AVR

Case 2: SG with AVR IEEET1 (DC type)

Case 3: SG with AVR IEEET2 (DC type)

Case 4: SG with AVR IEEET3 (DC type)

Case 5: SG with AVR EXAC1 (AC type)

Case 6: SG with AVR EXAC2 (AC type)

Case 7: SG with AVR EXAC3 (AC type)

Additionally, the setting of the DFIG operation was also simulated and investigated. There are two types of operations; firstly, the DFIG only injects active power, and second, it injects active power and performs reactive power management. The DFIG bus was modeled as a PQ bus for the first case, while it was modeled as a PV bus for the second case. For this scenario, the SG used an AVR with the IEEET1 type. As aforementioned, there are two cases in the wind plant operation type, namely:

Case A: DFIG as PQ Bus

Case B: DFIG as PV Bus

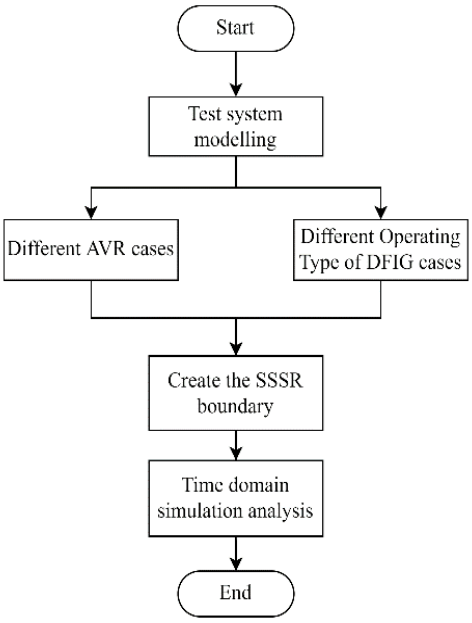

Fig. 6. Simulation scenarios.

This study used Case 1 and Case A as the initial conditions. Figure 6 depicts these conditions used as the initial condition in the "Different AVR Cases" and the "Different Operating Types of DFIG Cases." $P^{1}_{DFIG,i}$ demonstrates the active power value generated by the DFIG under conditions other than the initial cases, such as Case 2, Case 3, Case 4, Case 5, Case 6, Case 7, and Case B, at the i-test point.

Furthermore, this study gave the test system a small disturbance in the form of a generator torque increment of 1% at t=1s to verify its stability. This study presents the analysis by observing the system's condition through a time-domain simulation. To conclude, this study used this analysis to validate the results of the SSSR boundary.

4. RESULTS AND DISCUSSION

The modified method used to obtain the new SSSR boundary was implemented in various case studies. The first simulation was to establish the SSSR boundary of different types of AVR. The later simulation investigated how DFIG operation will impact the SSSR boundary. Both simulations were carried out because AVR and DFIG operating types have the same role in voltage control, so the impact on system stability can be quantified through this research.

4.1 Different AVR Cases

This research simulated and compared various AVR types using the modified method to obtain the SSSR boundaries. As stated earlier, the scenario ran seven cases, and the IEEE and EXAC AVR types were used in the simulations. The simulation aimed to determine how different AVRs affect the system's stability. The subsequent analysis discusses time-domain simulation to see how the system responds when a disturbance occurs. Furthermore, the time-domain simulation can be used to verify the modified SSSR boundary established.

4.1.1 The modified SSSR boundary for different types of AVR

In general, the SSSR boundary is produced when HB occurs, indicating instability in the system. However, this study created the boundary before the system experienced instability, guaranteeing stability to the outermost point on the boundary formed.

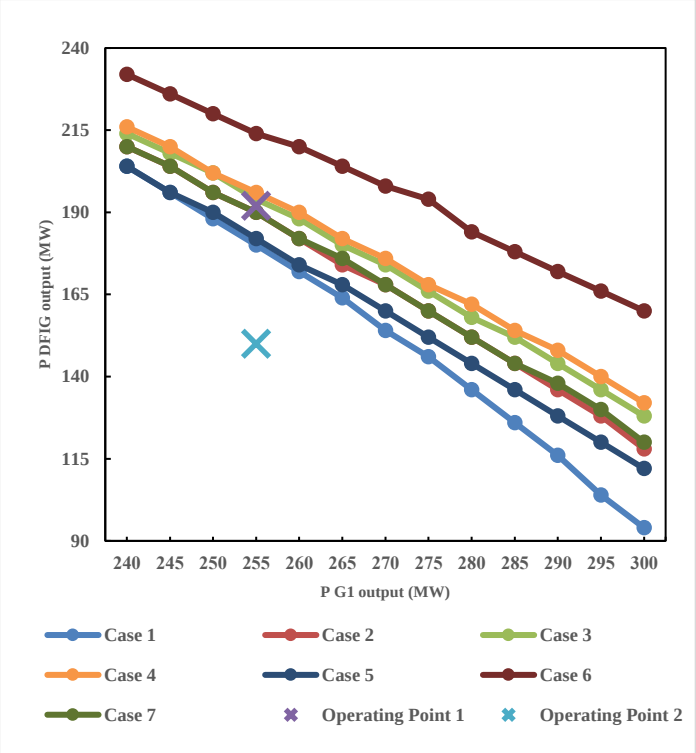

Fig. 7. The modified SSSR boundary with different types of AVR.

The modified SSSR boundary comprises a set of operating points of G1 and maximum DFIG power that guarantees the system's stability. The Appendix displays the maximum DFIG penetration corresponding to the G1 output power. The base case is Case 1, in which the synchronous generator G1 was without an AVR. In contrast, Case 2-7 is a G1 condition in which AVR had been implemented. Furthermore, the SSSR boundary in each case was compared to obtain the AVR type with the most extensive SSSR boundary, indicating a more stable system.

Figure 7 shows the modified SSSR boundary with various types of AVR. Compared to Case 1, the IEEE type (Case 2 to 4) had a more extensive SSSR boundary, with an increment of 10.7%, 15.4%, and 17.2% for Cases 2, 3, and 4, respectively. Following this, the EXAC type's boundary was also more extensive than Case 1, with an increment of 5.6%, 32.9%, and 11.3% for Cases 5, 6, and 7, respectively. After calculating the SSSR boundary increment, the following results were obtained: the most expansive and significant SSSR boundary for the IEEE and EXAC types were procured from the usage of Case 4 (IEEET3) and Case 6 (EXAC2), respectively. The use of EXAC2 produced the best performance compared to all the other observed cases, with a 32.9% increase in the SSSR boundary.

Figure 7 shows how the use of various types of AVR influences the power system's stability. When the output power of G1 (P G1) was 240 MW and the IEEET3 AVR type (Case 4) was being used, the maximum obtained penetration level of the DFIG (P DFIG) was 216 MW. However, the maximum penetration level can reach 232 MW if the SG utilizes EXAC2 type AVR (Case 6). These simulations show that various types of AVR lead to different system stability results.

This research presents a similar SSSR boundary pattern as previous studies [19], [20]. The SG output needs to be reduced to maintain stability when the DFIG penetration level is high. In earlier investigations, the HB occurrence was the operational point that composed the SSSR boundary. Also, previous studies show that the real eigenvalue may be positive since it might be zero or a very small positive value [19], [20]. This situation is critical, considering that the system's stability depends on the real part of the eigenvalue.

This study defines the operating point of the SSSR boundary by establishing the highest DFIG penetration level for every G1 output and ensuring the eigenvalue's real component is negative. This work guarantees that the system is in a stable condition. Tableble 4 shows the SSSR boundary operating point for AVR type IEEET3 (Case 4), confirming that each point has an eigenvalue with a negative real part.

Two operating conditions were selected to verify the SSSR boundary result. Operating point 1 was chosen at G1=255 MW and DFIG=192 MW, while operating point 2 was at G1=255 MW and DFIG=150 MW. Modal analysis was performed on various types of AVR using these two operation points.

Table **5.**le 5 shows the dominant eigenvalue for each AVR type. At operating point 1 (P G1 = 255 MW and P DFIG = 192 MW), four cases exhibited positive real parts of eigenvalues. This condition denotes that in Cases 1, 2, 5, and 7, the system was unstable at operating point 1. Figure 7 shows that operating point 1 (yellow cross sign) is outside the SSSR boundary in all four studied cases, which yields instability. Contrarily, in Cases 3, 4, and 6, the operating point 1 location is

within the SSSR boundary, resulting in a stable state for the system. Therefore, the point of operation should be operated inside the modified SSSR boundary to guarantee stability.

Table **5.**le 5 shows that operating point 2 results in a negative real part eigenvalue for all case studies, suggesting the system is stable. Figure 7 depicts the blue cross sign (operating point 2) within the SSSR boundary of all case studies, indicating the system is stable.

Table 4. Eigenvalue's dominant mode of SSSR boundary points for AVR type IEEET3.

	default method			modified method		
		eigenvalue			eigenvalue	
P G1 (MW)	P DFIG (MW)	real	imaginary	P DFIG (MW)	real	imaginary
240	218	0.0465	±j2.8141	216	-0.0255	±j2.9302
245	212	0.0626	±j2.797	210	-0.0092	±j2.9091
250	204	0.0092	±j2.8857	202	-0.0544	±j2.9965
255	198	0.0296	±j2.8604	196	-0.0347	±j2.9672
260	192	0.0521	±j2.8333	190	-0.0128	±j2.9361
265	184	0.0114	±j2.9034	182	-0.0474	±j3.0043
270	178	0.0379	±j2.8693	176	-0.0221	±j2.9662
275	170	0.0057	±j2.927	168	-0.0493	±j3.0216
280	164	0.0361	±j2.8869	162	-0.0204	±j2.9774
285	156	0.0113	±j2.9326	154	-0.0413	±j3.0207
290	150	0.0457	±j2.8874	148	-0.0084	±j2.9715
295	142	0.0275	±j2.9221	140	-0.0236	±j3.0037
300	134	0.0138	±j2.9504	132	-0.0348	±j3.0294

Table 5. Eigenvalue's dominant mode with different AVR cases.

Operating Point			Case	Eigenvalue	
No	G1 (MW)	DFIG (MW)		Real	Imaginary
1	255	192	1	0.0706	0
			2	0.0124	±3.5038
			3	-0.0464	±3.4409
			4	-0.0763	±0.0755
			5	0.1836	±3.1578
			6	-0.0768	±0.0754
			7	0.0221	±3.3199
2	255	150	1	-0.0762	±0.0770
			2	-0.0758	±0.0755
			3	-0.0758	±0.0755
			4	-0.0758	±0.0755
			5	-0.0758	±0.0755
			6	-0.0759	±0.0755
			7	-0.0758	±0.0755

Figure 8 illustrates the compilation of dominant eigenvalues for each case at operating point 1. The red cross sign indicates that the real part of eigenvalues is positive, which makes the system unstable. Furthermore, the scenario experiencing this phenomenon was in Cases 1, 2, 5, and 7. On the other hand, Cases 3, 4, and 6 did not have a positive real part of eigenvalues. Each eigenvalue is marked with a black symbol to indicate that its real component is negative, showing that the system remained stable.

Figure 9 shows the compilation of dominant eigenvalues for each case at operating point 2. All cases remain stable for the second operating condition (G1=255 MW and DFIG=150 MW) because all the real parts of the eigenvalues acquired were negative.

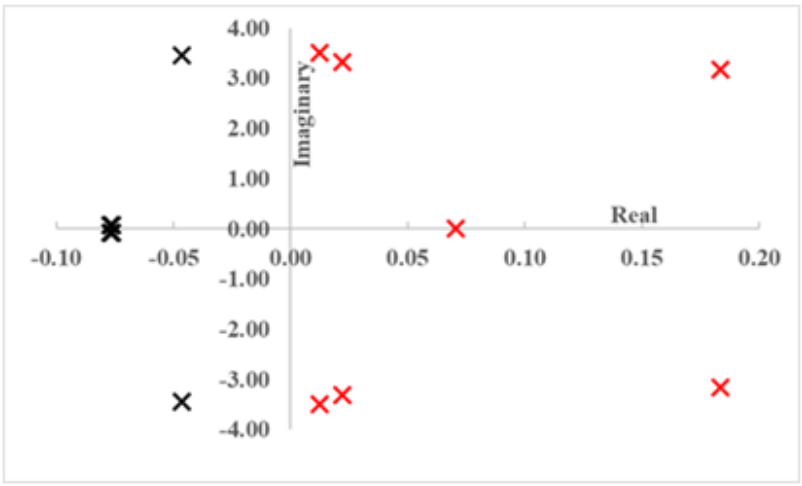

Fig. 8. Dominant mode of eigenvalues for operating point 1 in different AVR cases.

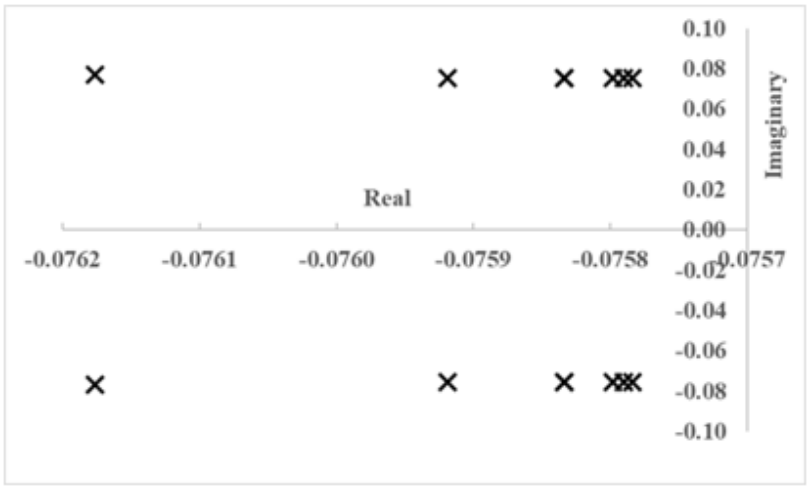

Fig. 9. Dominant mode of eigenvalues for operating point 2 in different AVR cases.

This simulation gives electricity operators a broad perspective on managing power generation to maintain stability. The system is stable if the operating point of the generators is inside the SSSR boundary. Conversely, instability occurs if the operating point of generators is outside the SSSR boundary.

4.1.2 Time-domain simulation for different AVR

The time-domain simulation is applied to show how the system performs when a disruption occurs. The disturbance in this research had a 1% increase in torque, i.e., t=1s, in the SG. Figure 7 shows the simulations carried out for the two operating points, showing G1 remaining at 255 MW while the DFIG output is at 192 MW and 150 MW.

The first time-domain simulation runs at operating point 1 (G1=255 MW and DFIG=192 MW). Figures 10 and 11 show the rotor angle output on IEEE and EXAC type AVR in time domain simulation, with small disturbance, respectively. The rotor angle appears to oscillate in Cases 2, 5, and 7 but can be damped in Cases 3, 4, and 6. Cases 2, 5, and 7 oscillated because the G1 could not dampen the disruption. This phenomenon also validates the created SSSR boundary. Furthermore, Figure 7 depicts that operating point 1 was outside the SSSR boundary of Cases 2, 5, and 7. However, in Cases 3, 4, and 6, the point of the operation was within the boundary, making it possible for the system to be adequately damped. Therefore, it can be concluded that the time domain simulation confirmed the created SSSR boundary.

Figures 12 and 13 show all the observed cases overcame the disruption in the second operating point (G1=255 MW and DFIG=150 MW). These results are because the operating point is within the created SSSR boundary. This simulation shows that when the system's operating point is within the SSSR boundary, even though experiencing small disturbances, the system can maintain its stability.

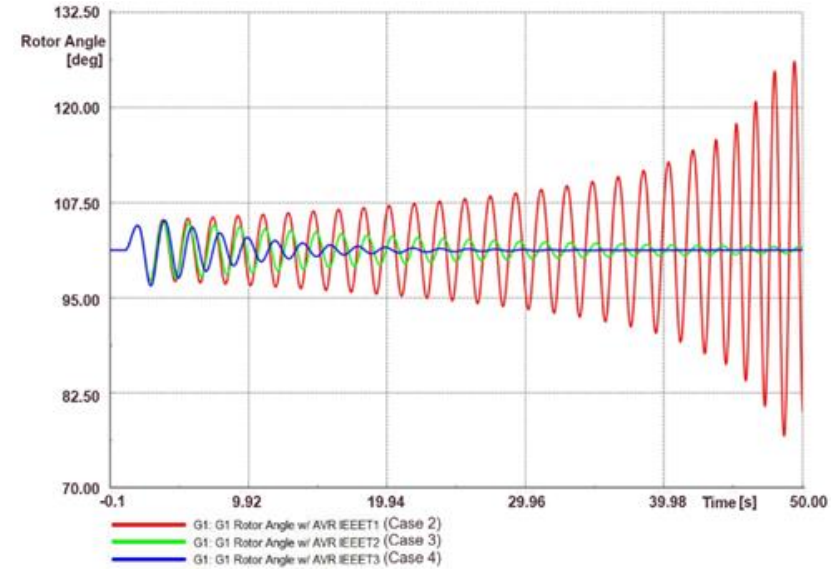

Fig. 10. Rotor angle on various AVR IEEE types at operating point 1.

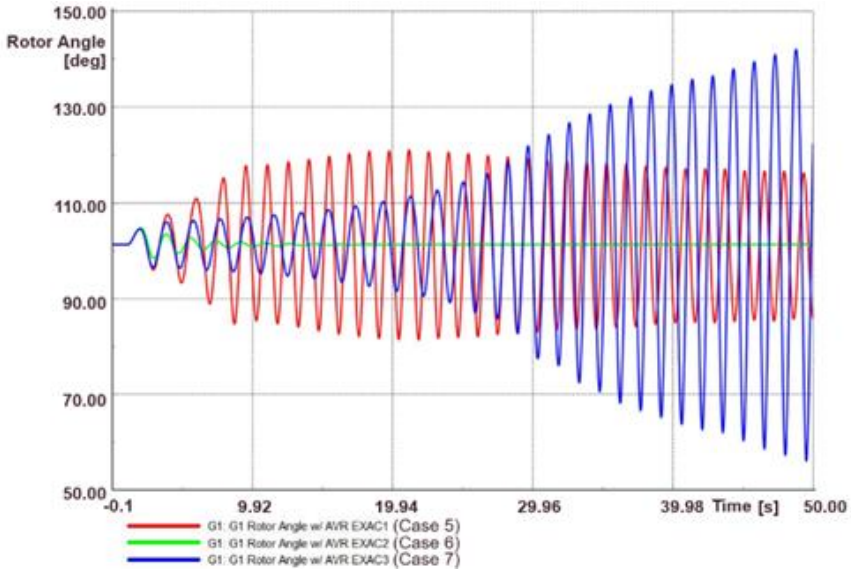

Fig. 11. Rotor angle on various AVR EXAC types at operating point 1.

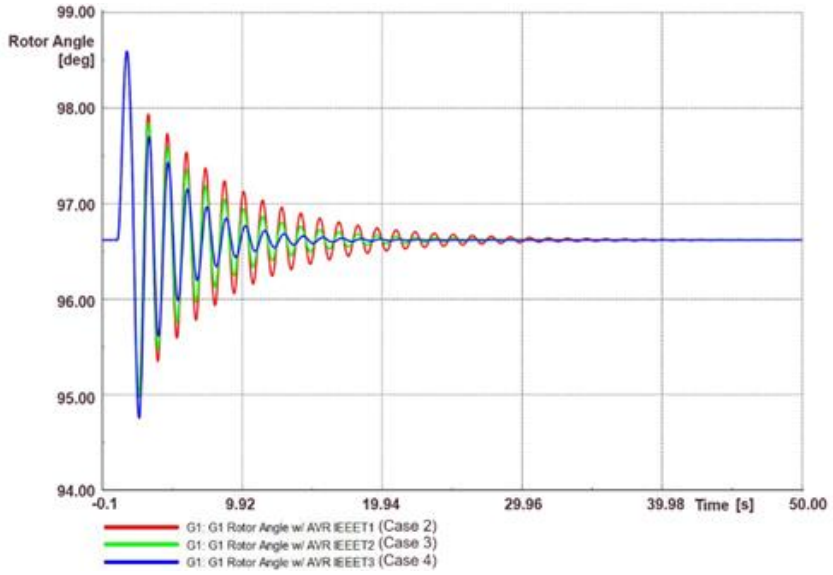

Fig. 12. Rotor angle on various AVR IEEE types at operating point 2.

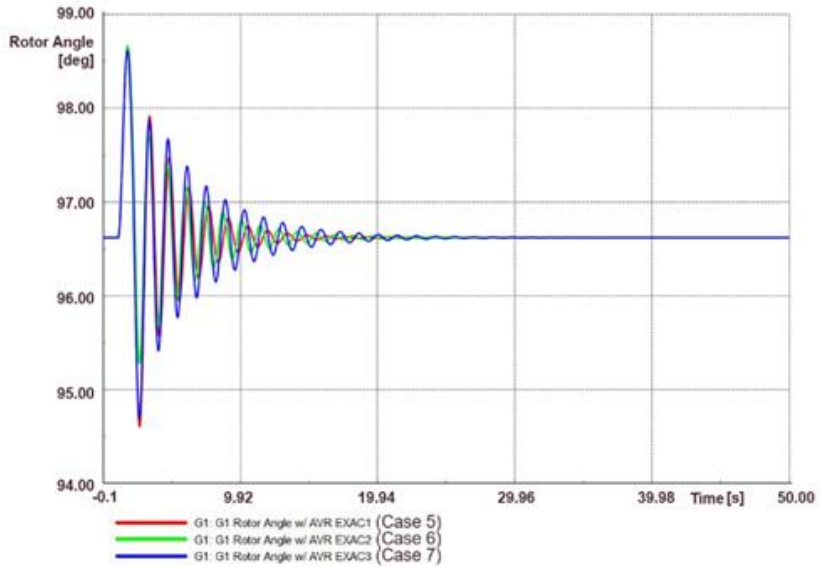

Fig. 13. Rotor angle on various AVR EXAC types at operating point 2.

This research is more comprehensive than earlier studies [10], [11] because it conducts the simulations at wide operating points. Research [10] examines the effects of using AVR on an electric power system with DFIG connected. However, this research [10] uses only one type of AVR. In contrast, this study uses different kinds of AVRs.

Research [11] compared various AVR types but only assessed stability analysis at one operating point. Meanwhile, this simulation examines the stability analysis at various range operations using two types of AVRs, namely IEEE and EXAC. This research discovers that EXAC-type AVR generates the best stability at various power plant operating points.

4.2 Different Operating Bus Types of DFIG

The DFIG's operating model can be described using the type of bus connection in the power system. When a DFIG is set as a PQ bus (case A), it will only inject active power and not contribute to reactive power. Meanwhile, if the DFIG is designated as a PV bus (case B), it will be able to contribute reactive power while injecting active power.

4.2.1 SSSR boundary for different operating bus types of DFIG

Figure 14 shows the modified SSSR boundary of the system with different types of DFIG buses. The maximum penetration level of the DFIG for each G1 output can be determined using the developed SSSR boundary. For example, if G1 operates at 255 MW, in Case A (PQ bus), the maximum penetration of the DFIG will be 190 MW. For the same G1 output, the DFIG can operate up to 240 MW in Case B (PV bus). Figure 14 shows the SSSR boundary appears narrower when the DFIG bus is set up as a PQ bus (orange line) than when it is set up as a PV bus (blue line). The DFIG does not contribute reactive power when the DFIG bus is a PQ bus.

Meanwhile, when the DFIG bus type was a PV bus, the SSSR boundary increased to 46.12% on average. When DFIG can produce reactive power, it enhances the system's stability because it possesses the same ability as AVR in the SG. Therefore, the presence of reactive power generated by the DFIG expanded the small signal stability of the system.

Table **6.**ble 6 shows the dominant eigenvalue of each operating type at specific points. Case A had a positive real part eigenvalue at operating point 1 (255, 192 MW), meaning the system was unstable. However, the results acquired from Case B, as Table **6.**ble 6 shows, imply that the system remains stable. This stability is because operating point 1 is inside Case B's SSSR boundary but outside Case A's. Both cases have negative real parts eigenvalue at the second operating point (255,150 MW). This result is due to the location of the point, which is within the SSSR boundaries of both cases.

Figure 15 shows the compilation of the location of the dominant eigenvalues in the axis for each case at operating point 1. A black cross denotes a stable eigenvalue, while a red cross indicates an unstable eigenvalue. Accordingly, Figure 16 shows the location of the dominant eigenvalues at operating point 2. The system remained stable because all the values obtained were on the left side of the eigenvalue locus.

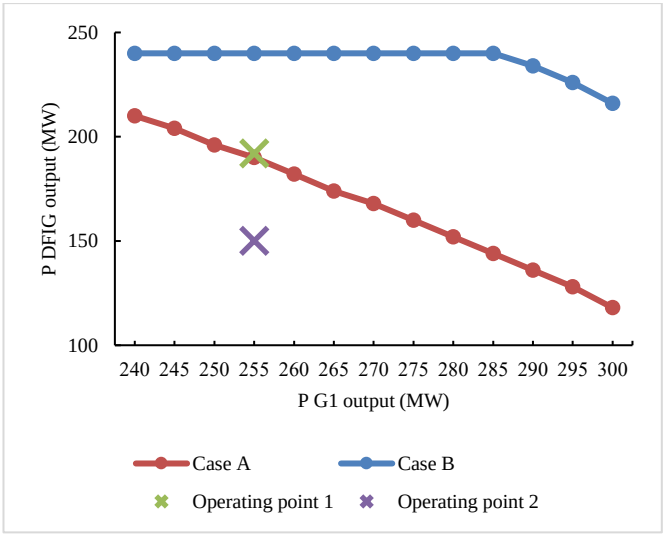

Fig. 14. SSSR boundary on different operating types of DFIG.

Table 6. Eigenvalue's dominant mode with different operating type DFIG cases.

Operating Point (MW)			Case	Eigenvalue	
No	G1	DFIG		Real	Imaginary
1	255	192	A	0.0124	+3.5038
			B	-0.0756	±0.0754
2	255	150	A	-0.0758	±0.0755
			B	-0.0756	±0.0754

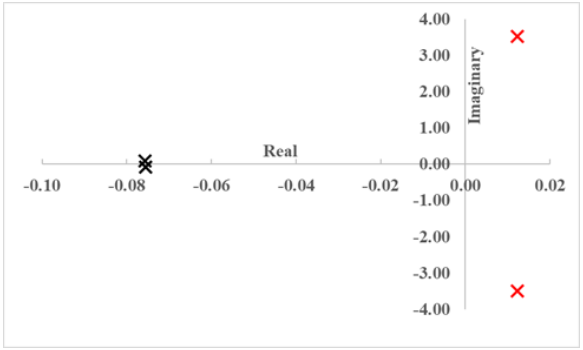

Fig. 15. Eigenvalue's dominant mode of different bus cases in operating point 1.

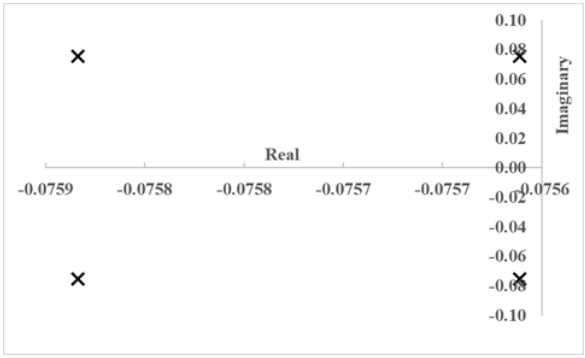

Fig. 16. Eigenvalue's dominant mode of different bus cases in operating point 2.

As confirmed in this simulation, how the DFIG bus is operated substantially impacts system stability. When DFIG is configured as PV buses, it can generate reactive power to networks; therefore, the resulting SSSR boundary is wider. By providing reactive power support, DFIG will improve the system's stability. In contrast, DFIG without reactive power support will reduce system stability.

4.2.2 *Time domain simulation for different bus types of DFIG*

The simulation in this section aims to discover the system response to a small disturbance at the operating point conditions of the SSSR boundary that have been obtained. Figure 14 shows that operating point 1 comprises the following values: G1=255 MW and DFIG =192 MW. In Case A (DFIG as PQ bus), the point of the operation was outside the SSSR boundary, but in Case B (DFIG as PV bus), it was inside the boundary. In this research, the disturbance was in a SG with a 1% torque increase at t = 1s. After applying the disturbance, the generator's rotor angle condition (G1) was observed.

Figure 17 depicts the rotor angle of G1 when the system was disrupted. This phenomenon occurred due to the different reactive power created in the two conditions. The DFIG did not provide any reactive power in Case A, which means that only G1 produced all of the system's reactive power in this case. In Case B, however, the DFIG provided reactive power; thus, the amount of reactive power provided by the G1 decreases. Consequently, the rotor angle's initial value differs between both cases.

Figure 17 also shows the rotor angle of G1 in Case B can quickly return to its stable state. In contrast, Case A keeps oscillating and does not return to its stability, thus, indicating instability. This simulation demonstrates that the DFIG's capacity to produce reactive power has a positive effect because its oscillation was well-dampened. By knowing this phenomenon, each generator operation point can be predicted using the SSSR boundary to avoid instability. Additionally, the stable region for both cases was investigated. One example was at operating point 2 (SG = 255 MW and DFIG = 150 MW), denoted by a yellow cross sign in Figure 14. The system oscillates when a slight disturbance occurs but is quickly damped. Figure 18 shows this phenomenon, and as a result, the established SSSR boundary is validated.

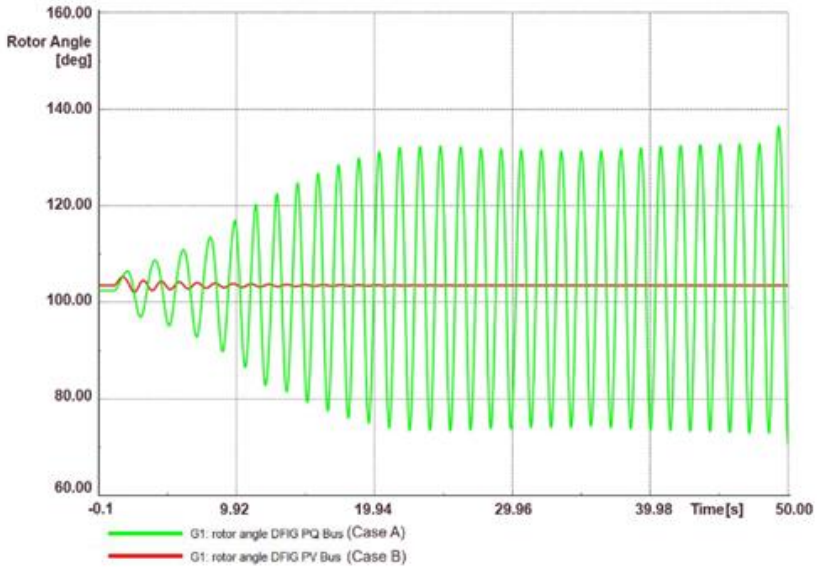

Fig. 17. Rotor angle of G1 on different operating type cases in operating point 1.

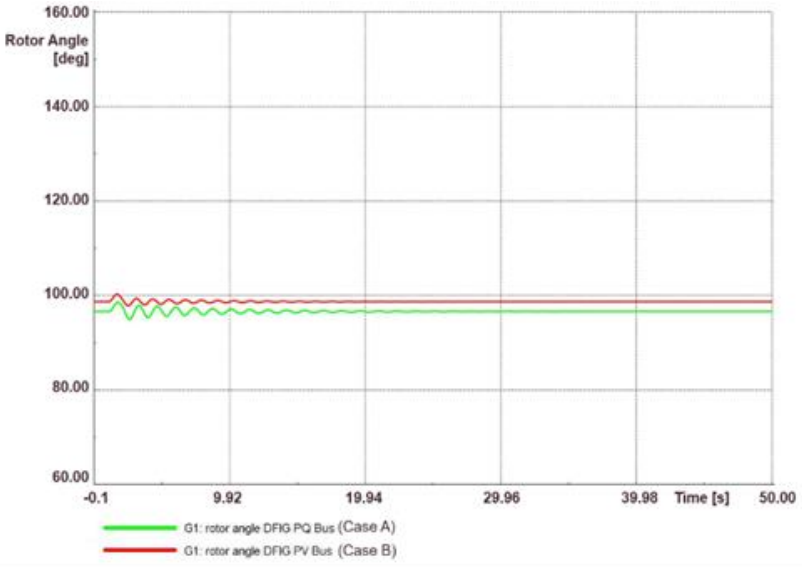

Fig. 18. Rotor angle of G1 on different operating type cases in operating point 2.

The DFIG's capacity to provide reactive power has demonstrated that it can effectively enlarge the SSSR boundary and damp oscillation. Furthermore, the DFIG wind turbine generator can be anticipated to supply both active and reactive power services as their penetration increases. Using the modified SSSR boundary method, electricity operators can more easily determine secure operating points, ensuring the system remains stable.

5. CONCLUSION

This study proposes a modified method for investigating the impact of wind power integration on the SSSR boundary. Operating points of the SSSR boundary were established by determining the highest DFIG penetration level for each SG output.

The modified method guarantees that the real parts of eigenvalues are negative; therefore, the system is stable. The proposed method has been successfully tested using a four-bus system. Boundary points of the SSSR have negative real parts of eigenvalues, thus guaranteeing a stable system.

Furthermore, this study investigated the effects of the SG AVR type and DFIG operation on the modified SSSR boundary. The investigation results show that AVR IEEET3 types could increase the SSSR boundary by 17.2%. Meanwhile, EXAC2 type 32.9% increased the SSSR boundary by, respectively, compared to the no-AVR condition. Therefore, the presence of AVR is essential for the system's stability.

Additionally, this study examined how the DFIG operating mode determines system stability. From the simulation results, when DFIG contributed reactive power to the system, the SSSR boundary increased by 46.12%.

This study also investigated the dynamic response of the system when a minimal disturbance occurs. The results show that the system oscillated when the power delivered by the DFIG and SG was outside the boundary. However, the disturbance could be damped when the delivered power was within the SSSR boundary. Admittedly, the developed modified SSSR boundary will assist utility operators in managing electricity from wind and conventional power plants.

The limitation of this study is that the observations were made using a simplified system. In addition, the AVR types used were limited to IEEE and EXAC types with a built-in parameter value from DIgSILENT PowerFactory. Research can be continued by implementing the modified method of SSSR boundary for other system configurations to assess the effect of wind energy penetration.

Additionally, the method for calculating the SSSR boundary should be improved by evaluating not only the real part of the eigenvalue but also the minimum damping ratio the system must be satisfied. This improvement is necessary so the system can be immediately damped when subjected to a disturbance. Furthermore, research related to additional DFIG control equipment for power system stability improvement is also needed.

APPENDIX

SSSR boundary points of G1 and DFIG.

G1 Output Power (MW)	DFIG Output Power (MW)								
	Case 1	Case 2	Case 3	Case 4	Case 5	Case 6	Case 7	Case A	Case B
240	204	210	214	216	204	232	210	210	240
245	196	204	208	210	196	226	204	204	240
250	188	196	202	202	190	220	196	196	240
255	180	190	194	196	182	214	190	190	240
260	172	182	188	190	174	210	182	182	240
265	164	174	180	182	168	204	176	174	240
270	154	168	174	176	160	198	168	168	240
275	146	160	166	168	152	194	160	160	240
280	136	152	158	162	144	184	152	152	240
285	126	144	152	154	136	178	144	144	240
290	116	136	144	148	128	172	138	136	234
295	104	128	136	140	120	166	130	128	226
300	94	118	128	132	112	160	120	118	216

ACKNOWLEDGEMENTS

This work was supported by Universitas Gadjah Mada under the Rekognisi Tugas Akhir (RTA) 2021 program.

REFERENCES

[1] Krasniqi G., Lajqi S., Đurin B., and Kranjčić N., 2022. Impact of installing small wind turbines in urban areas on reducing pollution – a case study. *International Energy Journal* 22(1): 49–60.

[2] Kouadria S., Berkouk E.M., Messlem Y., and Denaï M., 2018. Improved control strategy of DFIG-based wind turbines using direct torque and direct power control techniques. *Journal of Renewable and Sustainable Energy* 10(4): 043306.

[3] Dey P., Mitra S., Bhattacharya A., and Das P., 2019. Comparative study of the effects of SVC and TCSC on the small signal stability of a power system with renewables. *Journal of Renewable and Sustainable Energy* 11(3): 033305.

[4] Ngamroo I., 2017. Review of DFIG wind turbine impact on power system dynamic performances. *IEEJ Transactions of Electrical and Electronics Engineering* 12(3): 301–311.

[5] He P., Wen F., Ledwich G., and Xue Y., 2013. Small signal stability analysis of power systems with high penetration of wind power. *Journal of Modern Power Systems and Clean Energy* 1(3): 241–248.

[6] Ackermann T., 2012. *Wind Power in Power Systems*. West Sussex: Wiley.

[7] Li Z., Xu H., Wang Z., and Yan Q., 2022. Stability assessment and enhanced control of DFIG-based WTs during weak AC grid. *IEEE Access*, 10: 41371–41380.

[8] Gautam D. and V. Vittal, 2009. Impact of DFIG based wind turbine generators on transient and small signal stability of power systems. *IEEE Transactions on Power Systems* 24(3): 1426–1434.

[9] Vittal E., Malley M.O., and Keane A., 2009. A small-signal stability analysis of DFIG wind generation. In *Proceedings of 8th International Workshop on Large-Scale Integration of Wind Power into Power Systems, 14-15 October*. Bremen, Germany, 14-15 October. London: Energynautics.

[10] Mehta B., Bhatt P., and Pandya V., 2014. Small signal stability analysis of power systems with DFIG based wind power penetration. *International Journal of Electrical Power and Energy Systems* 58: 64–74.

[11] Essallah S., Bouallegue A., and Khedher A., 2019. Integration of automatic voltage regulator and power system stabilizer : small-signal stability in DFIG-based wind farms. *Journal of Modern Power Systems and Clean Energy* 7(5): 1115–1128.

[12] Fernández R. D., Mantz R.J., and Battaiotto P.E., 2007. Impact of wind farms on a power system. An eigenvalue analysis approach. *Renewable Energy* 32(10): 1676–1688.

[13] Hughes F.M., Anaya-lara O., Jenkins N., and Strbac G., 2006. A Power System Stabilizer for DFIG-Based Wind Generation. *IEEE Transactions on Power System* 21(2): 763–772.

[14] Farah A. and K. Alqunun. 2021. A new design method of PSS for power system including DFIG-based wind turbines. In *Proceedings of 12th International Renewable Engineering Conference, IREC 2021*. Amman, Jordan, 14-15 April. New York: IEEE.

[15] Zhao Z.L., Liu W.Y., and Bin Han X., 2013. Study on small signal stability improvement by PSS of the large-scale wind power integration. *International Journal of Computer and Electrical Engineering* 5(2): 2–5.

[16] Iorgulescu M. and D. Ursu. 2017. Reactive power control and voltage stability in power systems. In N.M. Tabatabaei, A.J. Aghbolaghi, N. Bizon, and F. Blaabjerg ed. *Reactive Power Control in AC Power Systems: Fundamentals And Current Issues*. Cham: Springer, 2017, pp. 227–248.

[17] Qin C., Zeng Y., Yang Y., Cui X., Xu X., and Li Y., 2017. Security region-based small signal stability analysis of power systems with FSIG based wind farm. In *Proceedings of 2nd Int. Conf. on Energy Engineering and Environmental Protection, EEEP 2017*. Sanya, China, 20-27 November. Philadelphia: Institute of Physics Publishing.

[18] Pan Y., Mei S., Liu F., and Wei W., 2016. Admissible region of large-scale uncertain wind generation considering small-signal stability of power systems. *IEEE Transactions of Sustainable Energy* 7(4): 1611–1623.

[19] Liu W., Ge R., Li H., and Ge J., 2014. Impact of large-scale wind power integration on small signal stability based on stability region boundary. *Sustainability* 6(11): 7921–7944.

[20] Liu W., Ge R., Lv Q., Li H., and Ge J., 2015. Research on a small signal stability region boundary model of the interconnected power system with large-scale wind power. *Energies* 8(4): 2312–2336.

[21] Ma Q., Xie R., Wei W., Yang L., Wu D., and Mei S., 2020. The small-signal stability region for power systems with uncertain parameters. In *Proceedings of 10th Int. Conf. Power Energy Syst. ICPES 2020*, Chengdu, China, 25-27 December. New York: IEEE.

[22] Kundur P., 1994. *Power System Stability and Control*. New York: McGraw Hill Inc.

[23] Saritha K.S., Sreedharan S., and Nair U. A novel optimal control strategy for energy management in a hybrid microgrid system. *International Energy Journal* 23(2): 83–96.

[24] Demirbas S. and S. Bayhan, 2011. Grid synchronization of doubly fed induction generator in wind power systems. In *Proceedings of 2011 Int. Conf. on Power Engineering, Energy and Electrical Drives*. Malaga, Spain, 11–13 May. New York: IEEE

[25] Babu B. and S. Divya, 2017. Comparative study of different types of generators used in wind turbine and reactive power compensation. *IOSR Journal of Electrical and Electronics Engineering*. 2: 2320–3331.

[26] NEPLAN, 2013. Exciter models - Standard Dynamic Excitation Systems in NEPLAN Power System Analysis Tool. *Küsnacht ZH*: 1–185.

[27] IEEE Power and Energy Society, 2016. IEEE Recommended Practice for Excitation System Models for Power System Stability Studies. New York: IEEE.

[28] DIgSILENT GmbH, 2018. *Nine-bus System*.

Gomaringen: DIgSILENT GmbH.
[29] DIgSILENT GmbH, 2018. *DFIG Template PowerFactory 2018*. Gomaringen: DIgSILENT GmbH.
[30] DIgSILENT GmbH, 2018. *PowerFactory 2018 User Manual*. Gomaringen: DIgSILENT GmbH.